# Silicon Qubits

**Thaddeus D Ladd,** HRL Laboratories, LLC, Malibu, CA, United States
**Malcolm S Carroll,** Sandia National Laboratory, Albuquerque, NM, United States



## Motivation for Silicon Qubits

The first motivation for basing qubits on silicon is the obvious foundation of classical microelectronics. Although silicon quantum computers would operate in a fundamentally different way from classical computers – for example, at cryogenic temperatures – still the level of development in material quality, crystal growth, and fabrication methodologies for silicon is unrivaled by any other material in the world. Leveraging even a small fraction of the worldwide investment in silicon for qubit development could potentially put silicon-based qubits far ahead of other solid-state alternatives.

The second, less obvious reason for choosing silicon is the remarkably clean magnetic environment witnessed by spins in highly purified and isotopically enriched silicon material. Fortuitously, 95.3% of the naturally occurring isotopes of Si nuclei ($^{28}$Si and $^{30}$Si) are spin-0. These nuclei therefore have a "closed shell" of nuclear moments, providing no external magnetic field whatsoever. Add to this the possibility of intrinsic silicon with part-per-billion chemical quality and the system is remarkably close to "vacuum" with respect to magnetic noise properties.

The most dramatic experimental demonstrations of this "semiconductor vacuum" are from inductively and optically probed magnetic resonance experiments in bulk silicon crystals which have been isotopically enriched to contain 99.9995% $^{28}$Si. These experiments probe dilute phosphorus impurities (at a density of $10^{15}$ cm$^{-3}$, i.e. one out of every 50 million atoms), which serve as donors in the material. For conduction electrons, these are closely analogous to a suspended single-charged ion, although it is worth recalling that these "ions" are suspended in a highly quiet material featuring negligible motion due to lattice vibrations without any need for laser cooling, laser trapping, or electrodes, in contrast to trapped ion or neutral atom qubit experimental setups.

In cryogenic, electron spin resonance (ESR) experiments, electron spins precess in an applied magnetic field, kicked off by a microwave pulse. The spinning electrons dephase first and foremost due to quasi-static inhomogeneities in the local magnetic field, an effect readily reversed by spin-echo techniques, which periodically invert the relative phases accrued by static rotation speed differences. At high levels of enrichment (e.g., 99.9995% $^{28}$Si) and once inhomogeneity is removed as a source of dephasing, he most important term causing dephasing is the dipole-dipole couplings between the dilute phosphorus atoms themselves. By applying a magnetic field gradient, these dipole-dipole effects can also be reduced. In Tyryshkin *et al.* (2012), it is shown that electron spins may be estimated to precess in phase for nearly a minute in this material.

Phosphorus impurities are optically addressable as well. They have a hydrogen-like energy structure in the THz energy range, which is inconvenient for both electronics and optics, but still a noteworthy structure for qubit studies (Litvinenko *et al.*, 2015). They also feature a set of sharp optical transitions corresponding to the transition from an atomic-hydrogen-like neutral donor to a molecular-hydrogen-like bound excitonic state. These transitions are atomically sharp in isotopically enhanced silicon, enabling the ability to polarize and measure the hyperfine couplings to the spin of the $^{31}$P nucleus. Again using radio-frequency pulses to refocus dephasing effects from inhomogeneous magnetic fields, these nuclei can be observed to precess without loss of phase coherence for hours, including at room temperature (Saeedi *et al.*, 2013).

These bulk experiments are a testament to the capability to preserve spin coherence in silicon, and are not replicated in any other material. But while a "vacuum" may be an apt description for the magnetic environment seen by conduction electrons, unfortunately the electronic structure of silicon is not completely "vacuum"-like. The electron structure of crystalline silicon produces an indirect bandgap. The energy minima for electrons in the conduction band are not at crystal momentum $k=0$, but rather along the six crystalline axes of the cubic structure, providing an anisotropy quite unlike a vacuum. These sixfold degenerate minima of the conduction band are referred to as valleys, and their degeneracy poses a problem for qubits since they can represent an uncontrolled degree of freedom for electrons that prevents clean control of qubit states. For the phosphorus impurity, the neutral donor ground state is an equal superposition of valley states which is energetically separated from other states by an energy of 11.7 meV in unstrained bulk (Zwanenburg *et al.*, 2013). While this effectively breaks the valley degeneracy for this system, a further consequence is that the atomic-like structure of the zero-phonon donor-bound exciton transitions comes with an extreme optical inefficiency: decay of the donor-bound exciton state is dominated first by Auger recombination, in which excitonic recombination ionizes the impurity, and second by broad phonon-assisted transitions.

Valley physics is more severe for electrons bound by large, shallow potentials in planar silicon devices. The valley degeneracy is partially broken by tensile strain in heterostructure stacks or by vertical electrostatic confinement in close proximity to an oxide interface, but while these effects raise four of the six valley states by 10s to 100s of meV, the remaining two valley states are much closer to degenerate. The splitting of these last two valleys is determined by atomic-scale details of the structure and the magnitude of the vertical electric field; assuring a sufficiently large value of this splitting is a key design constraint in silicon qubits.

Within a given valley or valley superposition, conduction electrons in silicon are reasonably well described by an effective mass model, with an in-plane effective mass of $0.19m_0$. This number is substantially higher than in GaAs, an earlier material studied for

spin qubits, requiring much higher demands on the lithographic resolution of structures for trapping or controlling electrons relative to GaAs. These limits are, however, within the limits of e-beam lithography and even modern implementations of photolithography. A substantial number of approaches to lithographically defined qubits have been introduced in the last 20 years. A technical review of many of these proposals and the progress on implementing them was compiled by Zwanenburg *et al.* (2013).

In this article, we highlight what the authors consider three of the most important categories of silicon qubits for silicon-based quantum computing, most of which have made substantial progress in demonstrating coherent operation since the Zwanenburg *et al.* review was published. These three principle categories of qubits are single phosphorus impurities, metal-oxide-semiconductor (MOS)-based dots, and dots based on heterostructures of strained silicon quantum wells with SiGe barriers. In what follows we will elaborate on these three essential categories, followed by categorization of the ways of controlling these qubits.

## Three Principal Material Types of Silicon Qubits

The three qubit categories are summarized in **Fig. 1**. All three types ultimately rely on the spins of trapped conduction electrons, although most variations of phosphorus-based qubits heavily employ the $^{31}$P nuclear spin as well. The first principle difference is the choice for how to confine electrons in the $z$-direction, defined as the substrate growth direction, normal to the silicon wafer. In the case of phosphorus impurities, it is the Coulomb attraction of the phosphorus impurity, which appears positively charged when replacing a silicon atom. This potential strongly attracts the electron, resulting in a binding energy of 45.6 meV (Zwanenburg *et al.*, 2013). In contrast, metal-oxide-semiconductor (MOS) quantum dots trap electrons in an electric potential defined by the hard "wall" of an oxide and the electric field created by the bending of the silicon bandgap due to the oxide interface. This potential is the same as that of the channel of a silicon MOS Field Effect Transistor (MOSFET), an extremely successful device forming the basis of modern microelectronics. The ground state of this approximately triangular potential sits at energies 10s of meV above the conduction band. SiGe quantum dots are similar to the MOS case, except in this system the barrier is pushed away from the surface of the semiconductor material, being defined instead by the band-offset between the strained silicon quantum well and a SiGe barrier, typically engineered to be larger than 150 meV (Zwanenburg *et al.*, 2013).

The trade-offs of the three approaches to vertical confinement have largely to do with disorder. A key advantage of the phosphorus system is that every phosphorus impurity provides effectively the same potential in a silicon lattice, assuming the impurity is sufficiently removed from surfaces or dielectric interfaces. This is in contrast to the quantum dot systems, where the exact energy of the vertical confinement may be impacted by random fluctuations in the amorphous oxide in the MOS case or by the heterostructure interface in the SiGe case.

A related distinguishing feature is the method for horizontal electron confinement. Here, the phosphorus system confines electrons horizontally in principally the same way as it does vertically: by its $1/r$ Coulomb potential. In contrast, the MOS and SiGe quantum dot systems rely on electrostatic gates to provide a horizontal potential profile for electrons. There are a number of strategies for designing these gates. Example scanning electron microscope (SEM), cross-sectional transmission electron microscope (TEM), and scanning tunneling microscope (STM) images of fabricated gates for all three vertical confinement types are shown in **Fig. 2**.

Most recent silicon quantum dot qubits are enhancement-mode devices, which are designed for an empty MOS or quantum well channel. A global field gate or individual dot gates pull the confined electrons from ohmic contacts. This contrasts with depletion mode structures, more typical in the AlGaAs/GaAs system, in which the system is doped such that a gas of electrons would reside in the channel region in equilibrium, but then negatively biased gate electrodes push electrons away from the dot regions, leaving behind a controlled number of charges. Depletion mode behaves poorly in silicon due to the disorder created by the dopants, which is more poorly screened in silicon than in GaAs. Besides avoiding disorder, however, enhancement-mode

| Type | Sketch | Main advantage | Main challenge |
|---|---|---|---|
| Donor | 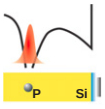 | Lowest disorder and largest valley splitting | Multi-qubit fabrication and operation |
| MOS | 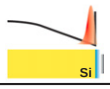 | Most similar to commercial transistors | Disordered potential |
| SiGe | 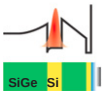 | Clean epitaxial barrier (low disorder) | Valley degeneracy |

**Fig. 1** Table indicating the three principle types of silicon qubits; the sketch column gives a rough image of the band structure as a black line, the electron wave function in red, and the material stack below. The confinement illustrated is referred to as "vertical" in the text (i.e. it the confinement in the growth direction), however the growth stack is here drawn horizontally, so that the energy of the band-structure above may be drawn vertically.

devices have the advantage that they could in principle confine electrons using only a single gate per dot. Most architectures mix enhancement and depletion operation using multiple gates per qubit. These multiple gates are useful for crafting each electron's confining potential, in part to overcome the effects of disorder in the vertically confining structure and in part to improve flexibility of electron control.

For all three silicon qubit categories, at least one form of control – under strong consideration since the seminal proposals of Loss and DiVincenzo (1998) for quantum dots and Kane (1998) for phosphorus donors – is the kinetic exchange interaction. This interaction relies on the ability to tune the energy level of a dot or donor based on a gate directly above it (called the A-gate in the Kane proposal and in this article, but often referred to as a plunger gate), and to control the interaction between nearby spins either via A-gates or with an additional gate controlling a tunnel barrier between the dots (called the J-gate in the Kane proposal and in this article, but often referred to as an exchange gate).

The kinetic exchange interaction is a consequence of quantum tunneling in the Coulomb blockade regime and Pauli exclusion (Zwanenburg *et al.*, 2013). The essential physics is that the spin-singlet state of a pair of electrons (with total angular momentum $S=0$ and an antisymmetric spin state) is capable of tunneling into the ground state for two electrons on a single dot or donor site, since the resulting state is fully antisymmetric. Spin-triplet states (with total angular momentum $S=1$ and a symmetric spin state) would, in contrast, result in a disallowed symmetric doubly-occupied ground state, and are therefore forbidden from tunneling unless the dots are detuned in energy by a sufficient amount to allow tunneling into excited orbital or valley states. The kinetic exchange interaction lowers the energy of the singlet state relative to the triplet state due to the singlet's allowed tunneling process. Electrical control of tunneling via gate voltages modulate this interaction, either by increasing the tunnel coupling directly (via J-gates) or by bringing the chemical potentials of the quantum dots or donors closer to a resonance condition (via A-gates).

Kinetic exchange provides one of the key proposed mechanisms for coupling silicon qubits, but there are others which will be addressed later in this article. Nonetheless, we will frame our discussion in terms of the basic A-gate/J-gate control of quantum dot chemical potentials and exchange energies for the sake of a meaningful comparison of the three basic categories. **Fig. 2(a)** provides the simplest visual realization of the A/J or plunger/exchange gate concept, with the visible "paddle" gates intending to serve the role of A gates and the straight gates between intending to serve the role of J gates. While harder to see in those images of dot-based devices employing overlapping gates, similar A/J functionality, in addition to horizontal confinement, is intended here as well.

Due to their naturally occurring confining potentials, phosphorus impurities would appear to have an advantage relative to dots in that the requirement of multiple gates for horizontal confinement is relaxed. However, the phosphorus system can introduce substantially more strict fabrication requirements compared to quantum dots, especially in multi-qubit systems. The phosphorus potential results in extremely small electron wavefunctions. The Bohr radius of an electron on a donor is approximately 2.5 nm. This means that in order to implement a reasonably strong exchange interaction entirely in the bulk, theory estimates that A-gates would need to be separated by approximately 10–20 nanometer pitch (Zwanenburg *et al.*, 2013). An additional challenge is that the nondegenerate phosphorus valley state creates a lattice-scale wavefunction oscillation, which results in a kinetic exchange interaction that varies from crystal-lattice site to crystal-lattice site (Zwanenburg *et al.*, 2013). Some early donor qubit designs, as a consequence, proposed extremely challenging donor and electrode placement, both vertically and horizontally (Hollenberg *et al.*, 2006; Testolin *et al.*, 2007).

Alternative long-range coupling schemes between donors, as we describe below when we elaborate on coupling mechanisms, might be employed to circumvent many of the strict requirements of exchange-based donor qubit architectures. Such approaches could use standard silicon foundry processing, using ion implantation to place an average number of donors within the placement requirements of these proposed schemes. For exchange-based donor approaches, however, a new fabrication technique with atom-scale precision is under parallel development. Using a scanning-tunneling-microscope (STM) to do lithography on a hydrogen-terminated Si surface, combined with exposure of the patterned surfaces to phosphine, a quasi-three-dimensional molecular-beam-epitaxy capability with spatial resolution at a single lattice site has been demonstrated (Fuechsle *et al.*, 2012). See **Fig. 2(h)** and **(i)** for qubit devices including both donor qubit islands and electrode gates fabricated this way (Watson *et al.*, 2015, 2017). The benefit of STM-defined phosphorus gates is not limited to their small size and pitch: the atom-by-atom fabrication leads to conducting channels that have shown substantially lower $1/f$ voltage noise than other lithographically defined gate stacks (Shamim *et al.*, 2016), which is a critical feature given that such $1/f$ noise may ultimately limit the fidelity of silicon qubits employing exchange interactions. The extremely promising and rapidly evolving STM-lithography approach, however, is still immature relative to the much more firmly established silicon foundry processes with respect to yield, integration, and manufacturing.

The appeal of quantum dot approaches relative to the phosphorus system is the engineering advantage of defining dots entirely by traditional lithography. The MOS system is especially promising in this regard due to its close affinity to the ubiquitous complementary-MOS (CMOS) transistor. A further advantage of MOS relative to the SiGe system is that the large vertical electric field present in this system breaks the valley degeneracy from a two-fold degeneracy to valley splittings that can easily exceed 300 $\mu$eV, corresponding to temperatures of 3.5 K (Gamble *et al.*, 2016). This large energy means that thermally initialized electron states have negligible excited valley population at typical dilution refrigerator temperatures. This vertical field is highly reduced in the SiGe system, leading to a less certain energy difference between the two lowest valley states. While comfortable valley splittings in excess of 50 $\mu$eV have been observed and used for high quality initialization, control, and read-out in some devices (Eng *et al.*, 2015), in other devices the valley splitting is too small for measurable qubit behavior (Borselli *et al.*, 2011; Zajac *et al.*, 2015).

Despite the challenge of valley splitting, the primary reason to consider SiGe-based dots relative to MOS-based dots has to do with noise and disorder. MOS-based dots place the qubit wavefunction against amorphous thermal $SiO_2$. While this is certainly the most developed and studied semiconductor-oxide interface in history, even the highest quality oxides have intrinsic interfacial

disorder. There is inherent atomic mismatch between the two materials. MOS transistors also routinely observe $1/f$ character trap noise. Oxide disorder, therefore, might have adverse impact on the yield of MOS dots and the $1/f$ noise may limit the fidelity of MOS-dot operation. Si/SiGe dots hope to reduce the effect of interfacial disorder by pushing the qubit wavefunction away from any oxide or metal interfaces and into a region of cleaner epitaxial crystalline semiconductor. Indirect measures of disorder such as mobility and the density at which transport is first observed (i.e., the metal insulator transition) are both appreciably lower in the strained-Si channels of the SiGe-based structures. A flexible gate design in MOS may enable tuning configurations to compensate for this difference in electrostatic disorder and indeed high quality single MOS dots have been demonstrated (Yang *et al.*, 2013). It is unclear whether this can be extended to bigger multi-dot networks. With respect to separation of the electron channel from imperfect amorphous interfaces with SiGe, to date, this has not completely eliminated the presence of $1/f$ noise, presumably coming from the remote gate and dielectric stack of the device. Recent measures of charge noise in MOS quantum dots (Freeman *et al.*, 2016) and recent qubits that include a MOS interface (Harvey-Collard *et al.*, 2017) show noise amplitudes comparable to

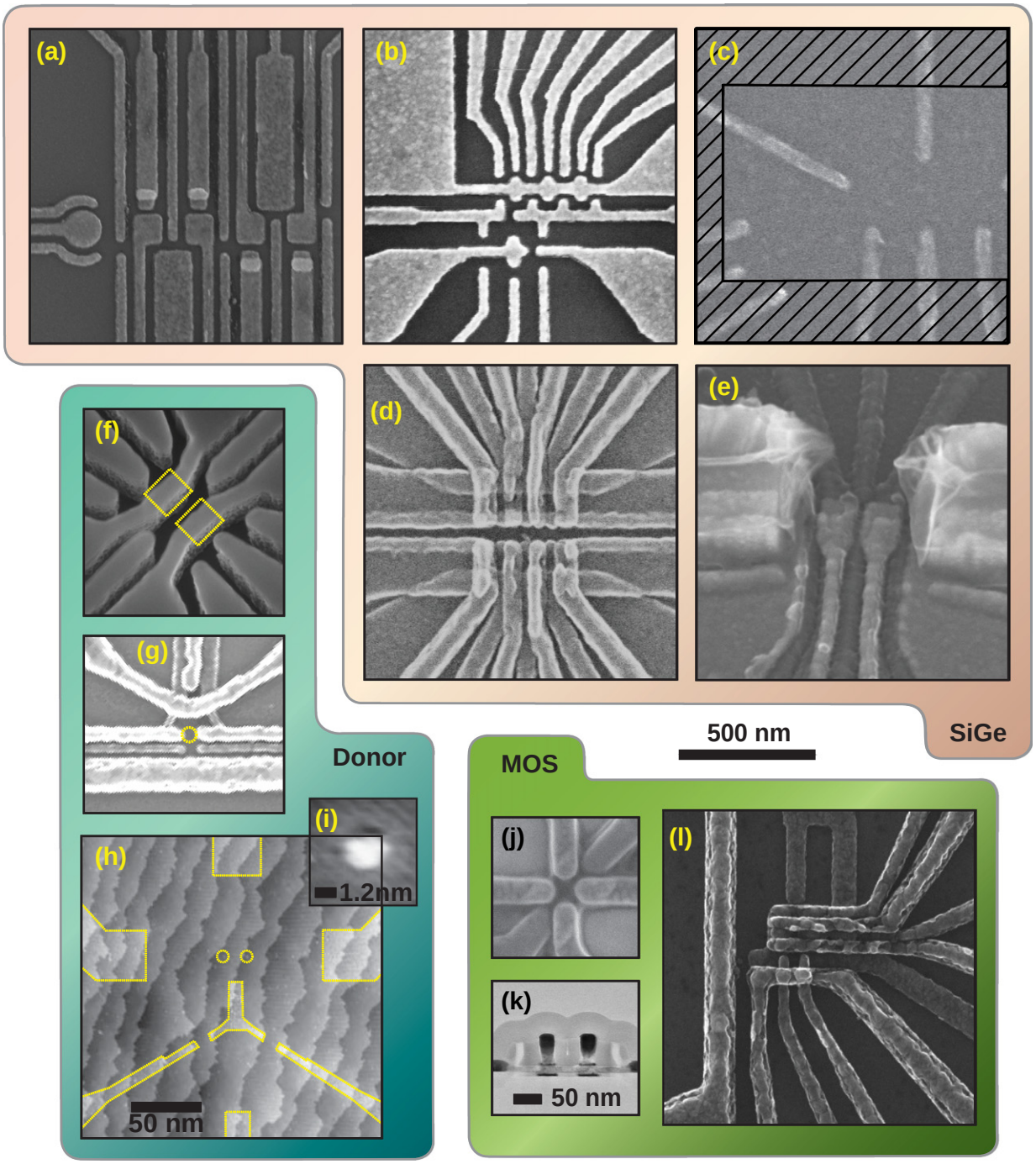

SiGe devices (Jock *et al.*, 2017). As of the date of this article, the relative performance of MOS vs. SiGe quantum dots relative to both interfacial disorder and charge noise remains unclear.

Following the choice of how to trap electrons, qubits are further defined by how those electrons are controlled. Again, there are a few principle strategies for defining and controlling qubits which we now define, noting that they are not exclusive, as well-engineered qubits are likely to use a combination of control mechanisms.

## Memory, Control, and Readout Mechanisms

Different types of silicon qubits make different choices for how to store quantum information, how to perform quantum logic, and how to read out quantum states. See **Table 1** for a summary of the qubit types which we detail below.

For memory, the first basic decision is whether to store information as charge or spin, the latter being by far the favored choice due to its much longer coherence time. However, when performing quantum logic, spin qubits are often partially converted to charge qubits. We therefore discuss both charge and spin qubits, and then proceed to indicate their control mechanisms.

### Charge Qubits

The simplest form of silicon qubit is the charge qubit. For this, consider two dots (or a dot and a donor) in charge states $(n,m)$ and $(n+1,m-1)$, where the two numbers indicate the number of conduction electrons or valence holes in each dot. The simplest such qubit would encode information on whether an electron is on the left dot (or donor) or the right, e.g. the charge states (1,0) and (0,1). A key motivation for this type of qubit is the simplicity of control, measurement and initialization. For control, direct modulation of gate voltages will reliably move charges between dots with speeds typically limited only by the control electronics employed. For measurement, single-electron-transistor or similar devices are capable of sensing the motion of single charges at low-temperature (Zwanenburg *et al.*, 2013; Gonzalez-Zalba *et al.*, 2015), enabling a direct read-out of this qubit's state. By sweeping voltage bias of confinement gates, broad ranges of charge numbers $n$ and $m$ can be detected by observing the tunneling of

**Table 1** Summary of memory and control mechanisms for silicon qubits discussed in this article.

<table>
<tr><th colspan="2">Memory</th><th>Single-qubit control</th><th colspan="2">Multiqubit control</th></tr>
<tr><td colspan="2">Charge</td><td>Direct charge motion</td><td rowspan="3">Capacative couplings</td><td rowspan="2"></td></tr>
<tr><td rowspan="4">Spin</td><td rowspan="2">Multi-spin</td><td>Exchange interactions</td></tr>
<tr><td>Single-triplet oscillations in gradients</td><td rowspan="3">Exchange and contact hyperfine interactions</td></tr>
<tr><td rowspan="2">Single-spin</td><td>ESR with AC magnetic fields</td><td rowspan="2">Magnetic dipole-dipole couplings</td></tr>
<tr><td>ESR with AC electric fields and gradients</td></tr>
</table>

**Fig. 2** Sample micrographs of silicon qubits. Qubits in the pink box employ SiGe heterostructures beneath the gate structures shown for gate confinement. Qubits in the blue box employ single donors. Qubits in the green box employ MOS confinement. All images are from SEMs except (h) and (i) which are STM images and (k) which is a TEM. All images are roughly scaled to the 500 nm scalebar shown in the center of the figure, except where indicated otherwise. Devices in Fig. (a)-(c) use Ti/Au gates, while those in (d), (e), (g), and (l) employ aluminum. Devices in (f) and (g) indicate windows for phosphorus donor implantation as dashed yellow regions. (a) Quadruple dot, image courtesy Mark Eriksson, University of Wisconsin, United States; simplified and adapted from Ward *et al.* (2016). (b) Triple dot structure fabricated by Christian Volk, Center for Quantum Devices, University of Copenhagen, 2016. (c). Double dot, image courtesy Kenta Takeda, University of Tokyo; see Takeda *et al.* (2016). doi: 10.1126/sciadv.1600694. The cross hatched region indicates the region in which a micromagnet made from deposited cobalt provides a magnetic gradient across the double-dot. A similar structure, without micromagnet, was demonstrated by HRL in Maune *et al.* (2012). (d) Six dot structure using overlapping gates, image courtesy Jason Petta, Princeton University; see Zajac *et al.* (2015). A similar structure was employed at HRL in Reed *et al.* (2016). (e) Double dot structure using overlapping gate with visible cobalt micromagnet. Image courtesy the Vandersypen group, copyright TU Delft, the Netherlands. (f) Polysilicon quantum dot and readout gate structure from Sandia National Laboratory; the quantum dot couples to an underlying phosphorus donor; see Harvey-Collard *et al.* (2017). (g) Gates for SET readout-channel for a single phosphorus device, courtesy Andrea Morello, UNSW; see Muhonen *et al.* (2014). (h) A phosphorus device in which both the qubit and the gates, outlined by dashed yellow lines, are fabricated by STM lithography. Courtesy of T.F. Watson from the Simmons Group, Center of Excellence for Quantum Computation and Communication Technology; see Watson *et al.* (2015). (i) A zoom into the yellow circle of the device in (h). (j) Quadruple quantum dot device in a fully depleted silicon-on-insulator (FDSOI) nanowire field-effect transistor. The gates shown are polysilicon separated by silicon nitride; electrons accumulate in corner states between the underlying silicon nanowire and an oxide surrounding them. Image courtesy Fernando Gonzalez-Zalba, Hitachi Cambridge Laboratory; see Betz *et al.* (2016). (k) TEM of a CMOS nanowire in the source/drain direction; the central features are two gates made out of TiN/polysilicon on $SiO_2$ and Hf-based dielectric. They are surrounded by silicon nitride spacers. See Maurand *et al.* (2016). (l) Aluminum MOS triple-dot structure. See Veldhorst *et al.* (2014). Image courtesy Andrew Dzurak, UNSW.

single charges from nearby baths, enabling initialization into a single $(n,m)$ state. The tunneling amplitude between a pair of dots may be voltage-controlled via the energy detuning or the size of the electrostatic tunnel barrier between the dots; indeed driving voltages at different rates may enable any superposition of qubit states via voltage control and appropriately controlled Landau-Zener-Stueckelberg oscillations (Ward *et al.*, 2016; Gonzalez-Zalba *et al.*, 2016).

Charge qubits are often used to study basic properties of quantum dots (Wang *et al.*, 2013), as well as provide proving grounds for the electrostatic interactions which may provide controlled-logic gates between qubits. For example, Ward *et al.* (2016) indicates a controlled-phase gate between a pair of single-electron charge qubits defined in a Si/SiGe heterostructure, using the device layout shown in **Fig. 2(a)**.

The disadvantage of a charge qubit is its sensitivity to charge noise. Charge noise may result from any noisy electric field, which may originate from fluctuators in the materials used in the device (e.g. $1/f$ noise from dielectrics) or from the control gates (e.g. Johnson noise from control circuitry). While the magnitude of charge noise will vary quite a bit between devices and experimental set-ups, typical dephasing times of charge qubits due to charge noise is in the range of 0.1–10 nanoseconds (Zwanenburg *et al.*, 2013). Given typical constraints of the electronics used to control qubits, these timescales are simply too fast for high fidelity operation.

## Spin Qubits

A comparably simple qubit is the single-spin qubit. A single electron spin bound to a donor or to a quantum dot is naturally a two-level quantum system, corresponding to spin-up and spin-down. As a fundamental magnetic dipole, a bound spin-1/2 has no sensitivity to electric fields, and interacts only magnetically. In silicon and silicon heterostructures, conduction-band electrons have a $g$-factor very close to 2, indicative of the small bulk spin-orbit interaction in silicon. Spin relaxation times typically exceed seconds at reasonable magnetic fields (Zwanenburg *et al.*, 2013).

The key advantage of the single-spin implementation relative to charge-qubit implementations is access to the long coherence times as observed in bulk systems. Recently, a single phosphorus qubit with single-spin encoding, implemented in silicon isotopically enhanced to contain only 800 ppm $^{29}$Si, showed a static dephasing time of 270 μs, extended to a multiple-spin-echo decoherence time exceeding 30 s (Muhonen *et al.*, 2014), despite its proximity to the aluminum gates forming the readout mechanism (see **Fig. 2(g)**). Similarly, a single spin qubit in an MOS dot, similar to that in **Fig. 2(l)**, also in 800 ppm $^{29}$Si, showed comparable times with static dephasing of 120 μs extended to a multiple-spin-echo decoherence time of 28 ms (Veldhorst *et al.*, 2014). Single-spin control for this system inherits the high-fidelity control of spin-resonance, enabling single-qubit gates with 99.6% fidelity as measured by randomized benchmarking (Veldhorst *et al.*, 2014).

A key consideration for single-spin encodings is that they typically require a large magnetic field, and their control requires careful tracking of each spin's Larmor precession in order to achieve phase-synchronous control. Ultimately, some limit to qubit coherence will exist due to the stability of the applied magnetic field or of the local oscillator. It is possible to circumvent these issues while still maintaining the coherence of spin qubits by using multi-spin qubits, in which qubit states are encoded by the total angular momentum of a set of spins. For example, the two-spin singlet-triplet qubit encodes information in the total angular momentum $S=0$ (singlet) and $S=1$ (triplet) subspaces of the two spins. A three-spin encoding combines a singlet-triplet pair with a third spin, assuring a total angular momentum $S=1/2$; a four-spin encoding likewise assures a total angular momentum $S=0$. These encodings are used in a way which imposes a constant total projection of angular momentum for all qubit states. In this way the qubit spin states can be brought to degeneracy for use as memory, assuring that the states do not evolve any phases relative to one another due to any constant or globally fluctuating magnetic fields. For this reason these qubits are referred to as decoherence-free subspaces or subsystems (DFS) (DiVincenzo *et al.*, 2000).

*Spin Control by ESR and EDSR:* To control single-spins, an obvious option is to use magnetic resonance, in which a large static applied magnetic field is present and transverse microwave magnetic fields are applied resonant with the electron Larmor precession of about 28 GHz per tesla of applied field. A clear technical difficulty with this mode of operation is that the controlling microwaves will typically not be localized, affecting multiple spins at once. To circumvent this difficulty, individual spins must have their resonant frequency shifted relative to their neighbors. In phosphorus devices, such a shift is available from the longitudinal component of the gate-controlled hyperfine interaction with the $^{31}$P nucleus (Kane, 1998; Laucht *et al.*, 2015), enabling resonance shifts of order MHz for reasonable gate voltage variations. In MOS and SiGe devices, $g$-factor inhomogeneity has been shown to result from spin-orbit effects in the quantum dot barrier, enabling dot-to-dot and voltage-tunable $g$-factor variations again on the order of MHz (Kawakami *et al.*, 2014; Veldhorst *et al.*, 2015).

Even more localized microwave control is possible using electric dipole spin resonance (EDSR), in which magnetic field gradients via micromagnets or spin-orbit effects convert AC electric fields to magnetic fields. If a magnetic field gradient is present, then voltage-induced motion of the electron in that gradient may mimic the effect of transverse microwave fields, except with the clear advantage of maintaining localization to the electron undergoing spatial modulation. In SiGe devices, fabricated cobalt micromagnets have provided this gradient (Takeda *et al.*, 2016; Kawakami *et al.*, 2014), as shown in the devices of **Fig. 2(c)** and **(e)**. Another possibility here is the use of hole spins, which naturally have a stronger spin-orbit interaction in confined nanostructures such as that in **Fig. 2(k)**, enabling EDSR without additional gradients (Maurand *et al.*, 2016).

*Spin Control by Kinetic Exchange:* The kinetic exchange mechanism enables a conversion between charge qubits (including, unfortunately, sensitivity to charge noise) and spin-qubits. It does this by using voltages to attempt to generate a superposition of (2,0) and (1,1) charge states (reminiscent of the charge qubit), the amplitudes and energies of which are different for

Pauli-allowed spin singlets and Pauli-excluded spin triplets in the (2,0) state. This spin-to-charge conversion is useful since it enables initialization, control, and measurement of spin-qubits without requiring high magnetic fields or magnetic field gradients.

The action of kinetic exchange is to reduce the energy of a singlet, which may be considered a single-qubit control axis for multiple spins encoded in a DFS. For a pair of spins in a singlet-triplet qubit, this voltage-induced interaction may therefore be considered a rotation about the *z*-axis of the multi-spin qubit's Bloch sphere. To control other axes in this case, another mechanism is needed. Examples of successful introduction of a second interaction for the additional control axes are magnetic gradients, arising from either deliberately introduced magnetic field gradients (Takeda *et al.*, 2016), single nuclear spin (Harvey-Collard *et al.*, 2017), or an ensemble of nuclear spins (Maune *et al.*, 2012). The latter case has been a fruitful qubit implementation in the nuclear-spin-rich system of GaAs (Nichol *et al.*, 2017).

Remarkably, if DFS encodings are used employing at least three spins per qubit, the exchange interaction can provide universal quantum logic, including multi-qubit gates, with no other control mechanisms. This was shown in DiVincenzo *et al.* (2000), which shows a pulse sequence locally equivalent to controlled-phase for two three-spin encoded DFS qubits. More recently, pulse sequences have been found which provide exchange-only multiqubit control without any specification made on the *m*-quantum number for either qubit, potentially allowing operation in much lower magnetic fields (Fong and Wandzura, 2011). This exchange-only encoding works best in highly uniform magnetic fields, and is particularly important for silicon where nuclear-induced gradients may be made very small via the use of isotopic enhancement. The basic operation of exchange-only triple-dots qubits in 800 ppm $^{29}$Si, using a gate layout similar to that in **Fig. 2(d)**, has been demonstrated in Eng *et al.* (2015) and Reed *et al.* (2016). This encoded triple-dot spin qubit showed a $^{29}$Si-limited static dephasing time of 3 μs, extended via exchange echo to over 600 μs at high magnetic field (Eng *et al.*, 2015), with operational fidelity limited by charge noise (Reed *et al.*, 2016).

*Initialization and Readout of Spin Qubits*: While the inductive techniques of magnetic resonance are excellent and highly mature for control, the readout-mechanisms of traditional magnetic resonance are many orders of magnitude too insensitive. One effective way to initialize and measure a single spin is via spin-selective tunneling to or from a bath. In particular, if a bath of electrons has its Fermi energy set via voltage to be between the two Zeeman sublevels of the dot spin, one spin will have available states for tunneling and the other will not. This basic principle depends on operating at a field and temperature such that the electron Zeeman energy $g\mu_B B$ vastly exceeds thermal energy $k_B T$, where the temperature here is that of the electrons in the bath (including any noise introduced from electronics, etc.). This is reasonable at fields of about a tesla, which also corresponds to convenient microwave ESR control frequencies of 3–30 GHz. This method of measurement has been employed for single-shot single-spin qubits in MOS (Veldhorst *et al.*, 2015), phosphorus (Muhonen *et al.*, 2014; Watson *et al.*, 2017), and SiGe (Kawakami *et al.*, 2014) systems.

Multi-spin encodings enable initialization and measurement using the Pauli-blockade mechanism, which enables the preparation and detection of singlets of spin pairs. This mechanism depends on distinguishing spin-dependent electron tunneling regimes, which requires electron temperatures much less than any excited state in the system. For SiGe qubits, low-lying valley states can easily prohibit this type of measurement, but nonetheless Pauli-blockade singlet-triplet measurement has been demonstrated in both SiGe and MOS dots (Zwanenburg *et al.*, 2013). Attempts to partially circumvent the effects of small valley splitting by operating in a filled shell (i.e., (3,1)–(4,0) occupation) have also been shown in coupled donor-dot and multi-dot systems (Harvey-Collard *et al.*, 2017).

## Qubit Couplings and Hybridizations

Coupling of qubits is necessary for computation. Four predominant coupling mechanisms in silicon qubit device architectures are: (1) contact hyperfine between electron and nuclear spins, (2) capacitive or electric dipole coupling; (3) spin dipole coupling; and (4) kinetic exchange. Shuttling of electrons has been considered as a complementary function with coupling mechanisms for donors and quantum dots. This is especially of interest for short range mechanisms that can restrict layout flexibility such as exchange and contact hyperfine (Skinner *et al.*, 2003; Witzel *et al.*, 2015; Pica *et al.*, 2016). Shuttling of electrons through quantum dot networks has been experimentally demonstrated in GaAs (Baart *et al.*, 2016; Fujita *et al.*, 2017).

The selection of coupling mechanism has a strong influence on both the physical manifestation (e.g., layout and signal control) as well as performance (e.g., speed and dominant error sources). Coupling mechanisms, less obviously, also allow redefinition of the single qubit encoding through qubit hybridizations. Hybridizations often seek "the best of both worlds," circumventing a challenge of one of the principal encodings through merging properties of a second qubit's properties. The invention of the transmon for Josephson-junction-based qubits is an example of the extraordinary success that can come from hybridization (Houck *et al.*, 2009).

### Contact Hyperfine Interaction

The Fermi contact hyperfine interaction is ubiquitously important for both quantum dot and donor qubits because it is the dominant mechanism through which nuclear spins interact with the electron spin (i.e., either directly through a strong coupling to a $^{31}$P nucleus or through overlap with trace $^{29}$Si or $^{73}$Ge). The contact hyperfine term, therefore, plays a role in the Hamiltonian of any qubit leading to contributions to line width or resonant frequency. In donors for which the electron spin is the primary

encoded qubit, as discussed earlier, the contact hyperfine is used as a tuning mechanism through the Stark shift (Kane, 1998; Laucht *et al.*, 2015).

Alternatively, the nuclear spin of the phosphorus atom has been proposed as either the data or memory qubit in several computing schemes (for example see Kane (1998), Skinner *et al.* (2003), Hill *et al.* (2015), Witzel *et al.* (2015), Pica *et al.* (2016)), due to several important advantages: it features extremely long coherence times, it can be isolated from the electric environment when the donor is ionized, and very high fidelity NMR rotations are possible. Furthermore, it naturally occurs with 100% abundance as the spin-1/2 $^{31}$P isotope and it is a qubit that, therefore, cannot be lost (i.e., there is always a spin ½ system present). A strong coupling between the electron and a nucleus is "built-in" to the donor system, with a substantial amplitude of 117.53 MHz (Zwanenburg *et al.*, 2013). This provides a convenient spin-spin coupling to this long-lived quantum memory.

The Kane proposal (Kane, 1998) and many variations of it published since, have indicated device architectures using electrons to mediate interactions between donor nuclear spins through the contact hyperfine interaction, although of course all proposals further need a mechanism for donor-donor coupling either through shuttling or other mechanisms that we discuss below. It is also worthwhile to note that the hyperfine contact term has already enabled repeated quantum-non-demolition measurement of the nuclear spin, offering extremely high initialization and read-out fidelity, while magnetic resonance techniques offer excellent control fidelity (Muhonen *et al.*, 2014). As an example process exploiting these high fidelity operations, Bell inequality violations in this electron-nuclear system were recently demonstrated (Dehollain *et al.*, 2016).

### Spin Qubit Coupling with Exchange

In the highly influential Loss/DiVincenzo (Loss and DiVincenzo, 1998) and Kane proposals (Kane, 1998), the kinetic exchange interaction is used as the entangling mechanism between single-spin qubits. As the name suggests, this interaction "exchanges" spins, enabling a "full swap" if tuned to a $\pi$-pulse. Spin-information can be moved across a device by a series of such swaps. Of course, if pulsed for half the duration, spins may be entangled. The sqrt-SWAP interaction between a pair of spins provides maximal entanglement; a controlled-NOT (CX) or controlled-phase (CZ) gate could then be accomplished using two sqrt-SWAP gates, with the additional use of single-spin rotations implemented via the methods described in the previous sections. Alternatively, exchange in the presence of Zeeman inhomogeneity due either to micromagnetic gradient fields or $g$-factor inhomogeneity can provide a CZ gate. Two-qubit gates for single spin qubits were recently demonstrated this way in MOS dots (Veldhorst *et al.*, 2015) and SiGe dots (Watson *et al.*, 2017; Zajac *et al.*, 2017). Sensitivity to charge noise was observed, providing one of the key present challenges in improving control fidelity of this type of coupling in QDs.

Exchange is a short-range interaction of order of the size of the electron wavefunctions. A possible longer term challenge for quantum dots and an immediate challenge for donors is the lithographic layout of the dense packing of electrodes needed to control the tunnel couplings, establish electron occupation, and provide readout and initialization capabilities. More complex layouts, such as extensions from present 1D layouts to 2D layouts, introduces challenges for exchange based architectures (Veldhorst *et al.*, 2016; Vandersypen *et al.*, 2017). For direct coupling of donor electron spins, the lithographic challenge is exaggerated both because of the more tightly confined electron wavefunction in the bulk and because of crystal-orientation-dependent tunnel coupling strengths. An alternate approach to couple donors through ionizing or hybridizing the donor electron to a larger surface quantum dot state (Kane, 1998; Calderon *et al.*, 2009) has been proposed to ease the lithographic requirements; recent experimental validations in this direction demonstrate coherent donor-quantum-dot hybrids (Harvey-Collard, *et al.*, 2017).

Variations of multispin and charge qubit hybridization can enable a variety of possibilities. One example is an encoding that resembles the triple-dot exchange-only qubit, but employs three electrons in two dots. An excited valley-orbit state in one of the two-dots effectively provides the third state of exchange-only control, with its energy splitting acting as an effectively constant exchange interaction. One axis of control is provided by voltage-controlled exchange-like interactions, while the other is provided by this excited-state splitting. Despite relying on what is ultimately a charge-state splitting for one axis of control, the coherence in these qubits can be extended to time scales of microseconds at the cost of substantially slowing down the qubit rotation times (Thorgrimsson *et al.*, 2017). Another example combining exchange with single spin qubits is that single spin qubit encodings can be combined with the singlet-triplet-readout methods of exchange qubits to provide direct means to make the parity measurements associated with quantum error correction (Jones *et al.*, 2016; Veldhorst *et al.*, 2016).

### Capacitive and Electric Dipole Coupling

Charge qubits, as well as spin-qubit encodings with a charge qubit component, offer a natural long-range coupling scheme. The electric field created by charge displacement in one qubit can be used to control the state by displacing the charge of another qubit. At short range, this is effectively a quantum cross-capacitance effect; at larger distances, it has the character of an electric dipole-dipole coupling. Capacitive coupling has enabled multiqubit logic in silicon-based charge qubits, such as the one shown in **Fig. 2(a)** (Ward *et al.*, 2016). Multispin qubits may be coupled this way, for example between singlet-triplet qubits that exploit the dipole difference between the (2,0) and (1,1) charge states to influence a neighboring qubit's charge states. The approach has been successfully demonstrated with nearest neighbor qubits reaching approximately 90% entanglement fidelity in a GaAs system (Nichol *et al.*, 2017). The distance between the qubits was approximately 500 nm in this case providing a modest relaxation of space constraints compared to exchange coupling.

Such coupling mechanisms may be especially pertinent for donor-based systems, since exchange couplings are challenging to engineer in this system. In one proposal, the electric dipole of a phosphorus impurity is "stretched" by the action of an A-gate, enabling electric control of a long-distance dipole-dipole coupling. Since this long-range coupling has a weak spatial dependence in comparison to exchange, these coupling mechanisms may allow phosphorus to be fabricated through a controlled ion implantation process, with the inevitable placement straggle compensated for by gate calibration (Tosi *et al.*, 2017). An electric dipole may also be created through the combination of a phosphorus impurity and an exchange-coupled quantum dot above it. Coherent quantum dot coupling to a single donor potential has been recently demonstrated, including characterization of the charge noise in that system (Urdampilleta *et al.*, 2015; Harvey-Collard *et al.*, 2017). Key to the success of these electric dipole coupling approaches is assuring that the mechanisms which provide the charge sensitivity for long-distance coupling may be rapidly modulated to prevent undue decoherence from charge noise.

Capacitive couplings may be enhanced or lengthened using extra hardware. Increasing the coupling range using floating gates has been proposed (Trifunovic *et al.*, 2012), although the small predicted effects of dissipation in these gates awaits experimental validation. Superconducting coupling elements seem especially promising, since the coupling of charge qubit components of qubits and the management of charge noise have been well addressed in the superconducting qubit community. These ideas are beginning to be adopted by silicon qubits, and superconductors may offer a powerful spin-charge hybridization offering benefits such as longer-range coupling. Conversion of exchange qubits to charge qubits allow charge-induced coupling to microwave fields in superconducting resonators, providing rapid spin-spin interactions across a chip; the recently demonstrated strong coupling of a single electron charge qubit in a SiGe device to a superconducting resonator is a critical step in this direction (Mi *et al.*, 2017).

Electric dipoles with optical oscillation frequencies could enable optical connections between silicon qubits, which would be especially convenient for those applications in optical quantum communication requiring memory and quantum logic. Unfortunately, silicon's indirect bandgap drastically reduces this system's efficiency for most existing concepts for spin-photon entanglement employing near-bandgap excitons, as demonstrated in III-V semiconductors. However, optically efficient emitters do exist in silicon and may provide future qubits with practical optical interfaces; a recent proposal employing chalcogen donors is provided in Morse *et al.* (2017).

### Magnetic Dipole Coupling

One of the potential advantages of single spin encodings is the long decoherence times due to the relatively good decoupling from environmental factors like charge noise. One approach to fully realize the long coherence times of spins is to altogether avoid all coupling schemes that have a charge qubit component. The spin is a magnetic dipole and the magnetic dipole-dipole interaction therefore provides a mechanism of coupling qubits not subject to charge noise. A critical challenge in exploiting dipole-dipole couplings is that they are long-range and "always on," making scheduled control challenging. Also they are slow, typically requiring millisecond interaction times. Nonetheless, this mechanism is appealing to donors because the dipole-dipole coupling avoids the atomic precision fabrication requirement for exchange and a system may exploit the long memory times of $^{31}$P nuclear spins. An early proposal for dipole coupled donor quantum computing argues that using a long range "always on" component is manageable combined with $g$-factor tuning (de Sousa *et al.*, 2004). The Stark shift of the donor contact hyperfine and $g$-factor has been modelled (Rahman *et al.*, 2009) and Stark shifted resonant frequency have been experimentally demonstrated both in ensembles and single donor cases (Wolfowicz *et al.*, 2014; Laucht *et al.*, 2015). A more recent architecture proposes a more direct modulation of the dipolar interaction through use of precisely timed ionization and deionization of donors to control the magnetic dipole-dipole coupling, holding information on the associated $^{31}$P nuclear spins (Hill *et al.*, 2015). This can substantially reduce the complication of long range coupling. In another recent proposal, mechanical motion of a scanning stage of $^{31}$P modulates the dipole-dipole coupling strengths (O'Gorman *et al.*, 2016). Although these architectures no longer require atomic-scale placement and gating, they still depend on highly uniform energy levels for a regular array of gated donors and the two qubit rotations are slower because of the weaker interaction strengths.

## The Future of Silicon Qubit Systems

In this article, we have outlined three principal ways of fabricating single-electron silicon systems, and three principal ways of encoding qubits on those systems. These fabrication and encoding techniques can furthermore be hybridized and combined producing improved features. Obviously, a large amount of design space exists for constructing systems of silicon qubits, and it remains an active, worldwide area of research to optimize the many trade-offs between the many possibilities. At the time of writing, the largest published coherently coupled silicon qubit system contains only two entangled qubits, leaving a long road ahead to the size and scale required for fault-tolerant quantum computing. Many concepts have been proposed for ways to scale, although many fundamental demonstrations remain to be proven prior to assurance that any such scaling path will succeed. However, the incredible scaling success of classical silicon microprocessors based on CMOS provides continual and dramatic encouragement of the notion that once the basic problems of charge-noise limits in control fidelities and valley- or disorder-limits in device yield are solved, a viable path for scaling to a useful technology will be found.

## Acknowledgement

Sandia National Laboratories is a multimission laboratory managed and operated by National Technology and Engineering Solutions of Sandia, LLC, a wholly owned subsidiary of Honeywell International, Inc., for the U.S. Department of Energy's National Nuclear Security Administration under contract DE-NA0003525.

*See also*: Cavity QED

## References

Baart, T.A., *et al.*, 2016. Single-spin CCD. Nat. Nanotechnol. 11, 330.
Betz, A.C., *et al.*, 2016. Reconfigurable quadruple quantum dots in a silicon nanowire transistor. Appl. Phys. Lett. 108, 203108.
Borselli, M.G., *et al.*, 2011. Pauli spin blockade in undoped Si/SiGe two-electron double quantum dots. Appl. Phys. Lett. 99, 063109.
Calderon, M.J., Saraiva, A., Koiller, B., Das Sarma, S., 2009. Quantum control and manipulation of donor electrons in Si-based quantum computing. J. Appl. Phys. 105, 122410.
Dehollain, J.P., *et al.*, 2016. Bell's inequality violation with spins in silicon. Nat. Nanotechnol. 11, 242.
de Sousa, R., *et al.*, 2004. Silicon quantum computation on magnetic dipolar coupling. Phys. Rev. A 70, 052304.
DiVincenzo, D.P., *et al.*, 2000. Universal quantum computation with the exchange interaction. Nature 408, 339.
Eng, K., *et al.*, 2015. Isotopically enhanced triple-quantum-dot qubit. Sci. Adv. 1, e1500214.
Fong, B.H., Wandzura, S.M., 2011. Universal quantum computation and leakage reduction in the 3-qubit decoherence free subsystem. Quantum. Inf. Comput. 11, 1003–1018.
Freeman, B.M., Schoenfield, J.S., Jiang, H.W., 2016. Comparison of low frequency charge noise in identically patterned Si/$SiO_2$ and Si/SiGe quantum dots. Appl. Phys. Lett. 108, 253108.
Fuechsle, M., *et al.*, 2012. A single atom transistor. Nat. Nanotechnol. 7, 242.
Fujita, T., Baart, T.A., Reichl, C., Wegscheider, W., Vandersypen, L.M.K., 2017. Coherent shuttle of electron-spin states. npj Quantum Inf. 3, 22.
Gamble, J.K., *et al.*, 2016. Valley splitting of single-electron Si MOS quantum dots. Appl. Phys. Lett. 109, 253101.
Gonzalez-Zalba, M.F., Barraud, S., Ferguson, A.J., Betz, A.C., 2015. Probing the limits of gate-based charge sensing. Nat. Commun. 6, 6084.
Gonzalez-Zalba, M.F., *et al.*, 2016. Gate-sensing coherent charge oscillations in a silicon field-effect transistor. Nano Lett. 16, 1614.
Harvey-Collard, P., *et al.*, 2017. Coherent coupling between a quantum dot and a donor in silicon. Nat. Commun. 8, 1029.
Hill, C.D., *et al.*, 2015. A surface code quantum computer in silicon. Sci. Adv. 1, e1500707.
Hollenberg, L., *et al.*, 2006. Two-dimensional architectures for donor-based quantum computing. Phys. Rev. B 74, 045311.
Houck, A.A., Koch, J., Devoret, M.H., Girvin, S.M., Schoelkopf, R.J., 2009. Life after charge noise: Recent results with transmon qubits. Quantum Inf. Process 8, 105.
Jock, R.M., *et al.*, 2017. Probing low noise at the MOS interface with a spin-orbit qubit. arXiv:1707.04357.
Jones, C., *et al.*, 2016. A logical qubit in a linear array of semiconductor quantum dots. arXiv:1608.06335.
Kane, B.E., 1998. A silicon-based nuclear spin quantum computer. Nature 393, 133.
Kawakami, E., *et al.*, 2014. Electrical control of a long-lived spin qubit in a Si/SiGe quantum dot. Nat. Nanotechnol. 9, 666.
Laucht, A., *et al.*, 2015. Electrically controlling single-spin qubits in a continuous microwave field. Sci. Adv. 1, e1500022.
Litvinenko, K.L., *et al.*, 2015. Coherent creation and destruction of orbital wavepackets in Si:P with electrical and optical read-out. Nat. Commun. 6, 6549.
Loss, D., DiVincenzo, D.P., 1998. Quantum computation with quantum dots. Phys. Rev. A 57, 120.
Maune, B.M., *et al.*, 2012. Coherent singlet-triplet oscillations in a silicon-based double quantum dot. Nature 481, 344.
Maurand, R., *et al.*, 2016. A CMOS silicon spin qubit. Nat. Commun. 7, 13575.
Mi, X., *et al.*, 2017. Strong coupling of a single electron in silicon to a microwave photon. Science 355, 156.
Morse, K.J., 2017. A photonic platform for donor spin qubits in silicon. Sci. Adv. 3, e1700930.
Muhonen, J.T., *et al.*, 2014. Storing quantum information for 30 seconds in a nanoelectronic device. Nat. Nanotechnol. 9, 986.
Nichol, J.M., *et al.*, 2017. High-fidelity entangling gate for double-quantum-dot spin qubits. npj Quantum Inf. 3. 3
O'Gorman, J., *et al.*, 2016. A silicon-based surface code quantum computer. npj Quantum Inf. 2, 15019.
Pica, G., *et al.*, 2016. Surface code architecture for donors and dots in silicon with imprecise and nonuniform qubit couplings. Phys. Rev. B 93, 034306.
Rahman, R., *et al.*, 2009. Gate-induced g-factor control and dimensional transition for donors in multivalley semiconductors. Phys. Rev. B 80, 155301.
Reed, M.D., *et al.*, 2016. Reduced sensitivity to charge noise in semiconductor spin qubits via symmetric operation. Phys. Rev. Lett. 116, 110402.
Saeedi, K., *et al.*, 2013. Room-temperature quantum bit storage exceeding 39 minutes using ionized donors in silicon-28. Science 342, 830.
Shamim, S., *et al.*, 2016. Ultralow-noise atomic-scale structures for quantum circuitry in silicon. Nano Lett. 16, 5779.
Skinner, A.J., Davenport, M.E., Kane, B.E., 2003. Hydrogenic spin quantum computing in silicon: A digital approach. Phys. Rev. Lett. 90, 087901.
Takeda, K., *et al.*, 2016. A fault-tolerant addressable spin qubit in a natural silicon quantum dot. Sci. Adv. 2, e1600694.
Testolin, M.J., *et al.*, 2007. Robust controlled-NOT gate in the presence of large fabrication-induced variations of the exchange interaction strength. Phys. Rev. A 76, 012302.
Thorgrimsson, B., *et al.*, 2017. Extending the coherence of a quantum dot hybrid qubit. npj Quantum Inf. 3, 32.
Tosi, G., *et al.*, 2015. Silicon quantum processor with robust long-distance qubit couplings. Nat. Commun. 8, 450.
Trifunovic, L., *et al.*, 2012. Long-distance spin-spin coupling via floating gates. Phys. Rev. X 2, 011006.
Tyryshkin, A.M., *et al.*, 2012. Electron spin coherence exceeding seconds in high-purity silicon. Nat. Mater. 11, 143.
Urdampilleta, R.M., *et al.*, 2015. Charge dynamics and spin blockade in a dybrid double quantum dot in silicon. Phys. Rev. X 5, 031024.
Vandersypen, L.M.K., *et al.*, 2016. Interfacing spin qubits in quantum dots and donors – hot, dense and coherent. npj Quantum Inf. 3, 34.
Veldhorst, M., *et al.*, 2014. An addressable quantum dot qubit with fault-tolerant control-fidelity. Nat. Nanotechnol. 9, 981.
Veldhorst, M., *et al.*, 2015. A two-qubit logic gate in silicon. Nature 526, 410.
Veldhorst, M., Eenink, H.G.J., Yang, C.H., Dzurak, A.S., 2016. Silicon CMOS architecture for a spin-based quantum computer. arXiv:1609.09700.
Wang, K., Payette, C., Dovzhenko, Y., Deelman, P.W., Petta, J.R., 2013. Charge relaxation in a single electron Si/SiGe double quantum dot. Phys. Rev. Lett. 111, 046801.
Ward, D.R., *et al.*, 2016. State-conditional coherent charge qubit oscillations in a Si/SiGe quadruple quantum dot. npj Quantum Inf. 2, 16032.
Watson, T.F., *et al.*, 2015. High-fidelity rapid initialization and read-out of an electron spin via the single donor d-charge state. Phys. Rev. Lett. 115, 166806.
Watson, T.F., *et al.*, 2017. A programmable two-qubit quantum processor in silicon. arXiv:1708.04214.
Witzel, W.M., Montaño, I., Muller, R.P., Carroll, M.S., 2015. Multi-qubit gates protected by adiabaticity and dynamical decoupling applicable to donor qubits in silicon. Phys. Rev. B 92, 081407(R).
Wolfowicz, G., *et al.*, 2014. Conditional control of donor nuclear spins in silicon using Stark shifts. Phys. Rev. Lett. 113, 157601.

Yang, C.H., Rossi, A., Ruskov, R., *et al.*, 2013. Spin-valley lifetimes in a silicon quantum dot with tunable valley splitting. Nat. Commun. 4, 2069.
Zajac, D.M., Hazard, T.M., Mi, X., Wang, K., Petta, J.R., 2015. A reconfigurable gate architecture for Si/SiGe quantum dots. Appl. Phys. Lett. 106, 223507.
Zwanenburg, F.A., *et al.*, 2013. Silicon quantum electronics. Rev. Mod. Phys. 85, 961.
Zajac D.M., *et al.*, 2017. Quantum CNOT gate for spins in silicon. arXiv:1708.03530.